



Article

Multicycle Performance of CaTiO₃ Decorated CaO-Based CO₂ Adsorbent Prepared by a Versatile Aerosol Assisted Self-Assembly Method

Ren-Wei Chang^{1,2}, Chin-Jung Lin^{3,*}  and Ya-Hsuan Liou^{1,2,*}¹ Department of Geosciences, National Taiwan University, Taipei 106, Taiwan; d06224005@ntu.edu.tw² Research Center for Future Earth, National Taiwan University, Taipei 106, Taiwan³ Department of Environmental Engineering, National Ilan University, Yilan 260, Taiwan

* Correspondence: lincj@niu.edu.tw (C.-J.L.); yhliou@ntu.edu.tw (Y.-H.L.)

Abstract: Calcium oxide (CaO) is a promising adsorbent to separate CO₂ from flue gas. However, with cycling of carbonation/decarbonation at high temperature, the serious sintering problem causes its capture capacity to decrease dramatically. A CaTiO₃-decorated CaO-based CO₂ adsorbent was prepared by a continuous and simple aerosol-assisted self-assembly process in this work. Results indicated that CaTiO₃ and CaO formed in the adsorbent, whereas CaO gradually showed a good crystalline structure with increased calcium loading. Owing to the high thermal stability of CaTiO₃, it played a role in suppressing the sintering effect and maintaining repeated high-temperature carbonation and decarbonation processes. When the calcium and titanium ratio was 3, the CO₂ capture capacity was as large as 7 mmol/g with fast kinetics. After 20 cycles under mild regeneration conditions (700 °C, N₂), the performance of CO₂ capture of CaTiO₃-decorated CaO-based adsorbent nearly unchanged. Even after 10 cycles under severe regeneration conditions (920 °C, CO₂), the performance of CO₂ capture still remained nearly 70% compared to the first cycle. The addition of CaTiO₃ induced good and firm CaO dispersion on its surface. Excellent kinetics and stability were evident.

Keywords: CO₂ adsorbent; calcium oxide; multicycle performance

Citation: Chang, R.-W.; Lin, C.-J.; Liou, Y.-H. Multicycle Performance of CaTiO₃ Decorated CaO-Based CO₂ Adsorbent Prepared by a Versatile Aerosol Assisted Self-Assembly Method. *Nanomaterials* **2021**, *11*, 3188. <https://doi.org/10.3390/nano11123188>

Academic Editors: Maria Filipa Ribeiro and Fabrizio Pirri

Received: 19 October 2021
Accepted: 18 November 2021
Published: 24 November 2021

Publisher's Note: MDPI stays neutral with regard to jurisdictional claims in published maps and institutional affiliations.



Copyright: © 2021 by the authors. Licensee MDPI, Basel, Switzerland. This article is an open access article distributed under the terms and conditions of the Creative Commons Attribution (CC BY) license (<https://creativecommons.org/licenses/by/4.0/>).

1. Introduction

The global climate-change phenomenon has become an important concern in recent years because of excessive CO₂ emissions, and this situation will continue because our energy supply originates mostly from fossil-fuel combustion now and in the next few years. Therefore, capturing CO₂ from flue gas and transporting it to a suitable site for storage is a solution for CO₂-emission reduction [1–3]. Calcium is an abundant element on earth, and its oxide form, CaO, can capture CO₂ and change it to the carbonate form, CaCO₃, via carbonation. Then the oxide form can be regenerated back by CO₂ removal through decarbonation. Therefore, CaO-based adsorbents can be used repeatedly by combining carbonation and decarbonation processes [4–8]. The nontoxicity and low cost of CaO-based adsorbents also enable them to become excellent potential candidate for CO₂-adsorption application.

However, the sintering problem that causes CO₂-capture capacity loss dramatically after few cycles remains a challenge during operation in high-temperature environments (600–900 °C) [4,9–11]. The process of CO₂ capture by calcium oxide can be divided into two stages: the surface chemical-reaction controlled stage and the inner-diffusion-controlled stage [12,13]. The former has higher capture efficiency than the latter. The sintering effect increases particle size. Larger particle sizes result in the difficult use of inner calcium oxide because the latter stage is more important. Thus, the capture performance is reduced. Introducing additives with high thermal stability into CaO-based adsorbents has been a

common strategy to mitigate sintering effects and improve cyclic stability. This strategy involves adding another metal (Zr, Al, Mg, Si, etc.) precursor during CaO-based adsorbent preparation, and then high-thermal-stability additives form independently (e.g., MgO, Al₂O₃, SiO₂) or react with partial calcium (e.g., Ca₉Al₆O₁₈, CaZrO₃) as the sorbent is obtained [13–19], or introducing it into high-thermal-stability porous silica solid (e.g., SBA-15, KIT-6) via the impregnation process [9,20,21]. The granules form sorbents for enhancing mechanical stability, or acoustic sound-assisted technique are also considered to reduce sorbent deactivation after several repeated uses [22,23].

The incorporation of titanium additives can introduce calcium titanium oxide (CaTiO₃) into CaO-based adsorbents. This introduction can be expected to alleviate the CaO-based adsorbent sintering problem, owing to its thermal stability at the working temperature of CaO-based adsorbents [24,25]. Yu et al. used the precipitation and deposition method to prepare Ca/Al/Ti sorbents. The capture capacity was reduced less than 5% after 10 cycles of the capture–regeneration experiment as small amount of titania were introduced. Wu et al. prepared CaTiO₃/nano-CaO by the hydrolysis method. The authors found that the high melting point of CaTiO₃ can improve the cyclic stability of CaO-based adsorbents. The sorbent almost retained its capacity after 40 repeated uses.

Our scope is to prepare well sintering-resisted CaO-based CO₂ adsorbent through an easily scaled up process. In the current work, CaTiO₃-decorated CaO-based CO₂ adsorbent was prepared by the aerosol-assisted self-assembly method. This method can be used to quickly and continuously prepare multicomponent metal oxide [26,27]. The properties and CO₂-capture performance of sorbents with different calcium and titanium mole ratios were investigated.

2. Materials and Methods

2.1. Adsorbents Preparation

In the typical preparation, 11.5 mL of acetic acid (Nacalai, Nacalai Tesque, Kyoto, Japan, 99%), 5 mL of hydrochloric acid (Nacalai, Nacalai Tesque, Kyoto, Japan, 35%), 60 mL of alcohol (Nacalai, Nacalai Tesque, Kyoto, Japan, >99.5%), calcium nitrate 4-hydrate (Ca(NO₃)₃ · 4H₂O, Macron, Avantor Inc., Radnor, PA, USA), and 6 g of F127 (Sigma-Aldrich, Sigma Ltd., Saint Louis, MO, USA) were added in 17 mL of tetrabutyl orthotitanate (Ti(OC₄H₉)₄, Sigma-Aldrich, Sigma Ltd., Saint Louis, MO, USA, 97%) sequentially. The mole ratio of Ca(NO₃)₃ · 4H₂O to Ti(OC₄H₉)₄ was 1.2/2/3/5. The mixture was stirring until all chemicals totally dissolved. Then, the transparent mixture solution was transformed to aerosol by nozzle first, and then passed through a 400 °C furnace. The as-prepared product was collected on filter paper. The sorbent was obtained by calcination at 700 °C for 30 min with a 1 °C/min heating rate. The received sorbent was named as CaTi-x, where x represents the mole ratio of calcium to titanium.

2.2. Adsorption Characterization

An X-ray diffraction (XRD) measurement was completed by PANalytical X' Pert PRO (Cu Kα λ = 0.154 nm, voltage: 45 kV, current: 40 mA). A nitrogen adsorption/desorption experiment was completed by Micromeritics ASAP 2020 (degas condition: 130 °C overnight, analysis condition: liquid nitrogen environment). Surface area was calculated from the adsorption isotherm in the relative pressure range of 0.05–0.3 using BET theory. Scanning electron microscopy (SEM) was done using a JEOL JSM-6500F.

2.3. CO₂ Capture Experiments

CO₂ capture experiments were evaluated by the gravimetric method (TA SDT-Q600). Approximately 5 mg of sorbent was used and pretreated at 700 °C under pure nitrogen gas flowing for 0.5 h. The capture environment was set at 600 °C under pure CO₂ gas flowing for 1 h. A cyclic stability experiment was done by using the gravimetric method. Each cycle combined carbonation and regeneration processes, and a pretreatment process was added before the cycle experiment started. The capture condition was set at 600 °C under

pure CO₂ gas flowing for 5 min, and the regeneration condition was set at 700 °C under pure N₂ gas flowing for 50 min (20 cycles) and 920 °C under pure CO₂ gas flowing for 15 min (10 cycles).

3. Results and Discussion

3.1. Properties of Adsorbents

The SEM images of obtained sorbents with different calcium to titanium mole ratios are shown in Figure 1. Owing to fixed titanium precursor addition amounts, the larger ratio corresponded with more calcium-precursor loading. At low calcium-precursor loading (CaTi-1.2 and CaTi-2), the morphology showed a more aggregate pattern than high calcium-precursor loading (CaTi-3 and CaTi-5).

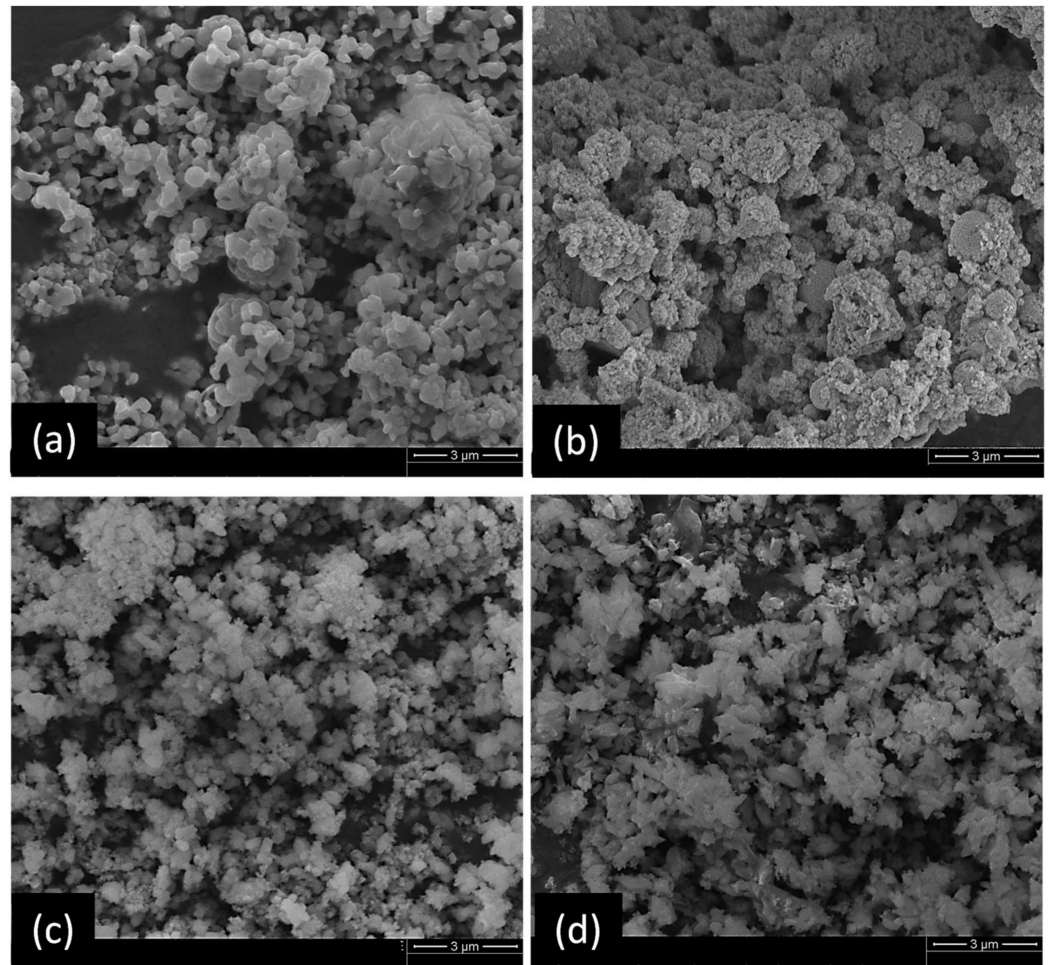


Figure 1. SEM images of as-prepared calcium-based sorbents: (a) CaTi-1.2, (b) CaTi-2, (c) CaTi-3, (d) CaTi-5.

The XRD result, as shown in Figure 2, revealed that CaTi-1.2 and CaTi-2 had diffraction signals assigned as CaTiO₃ contribution (JCPDS #220153) only. With increased calcium loading, the diffraction signals' intensities contributed by CaTiO₃ decreased. The CaO diffraction signal was not observed in the two sorbents because less calcium was available to form a highly crystalline structure. CaTi-3 presented diffraction signals contributed by CaTiO₃ and CaO (JCPDS #772376). The sample with higher calcium-precursor loading sorbent, CaTi-5, presented two other diffraction signals from Ca(OH)₂ (JCPDS #841263) compared with CaTi-3. This result indicated that only certain amounts of calcium can form high-thermal-stability oxide with titanium, and the others formed oxide itself. The highly crystalline hydroxide form demanded more calcium to participate than did the oxide form.

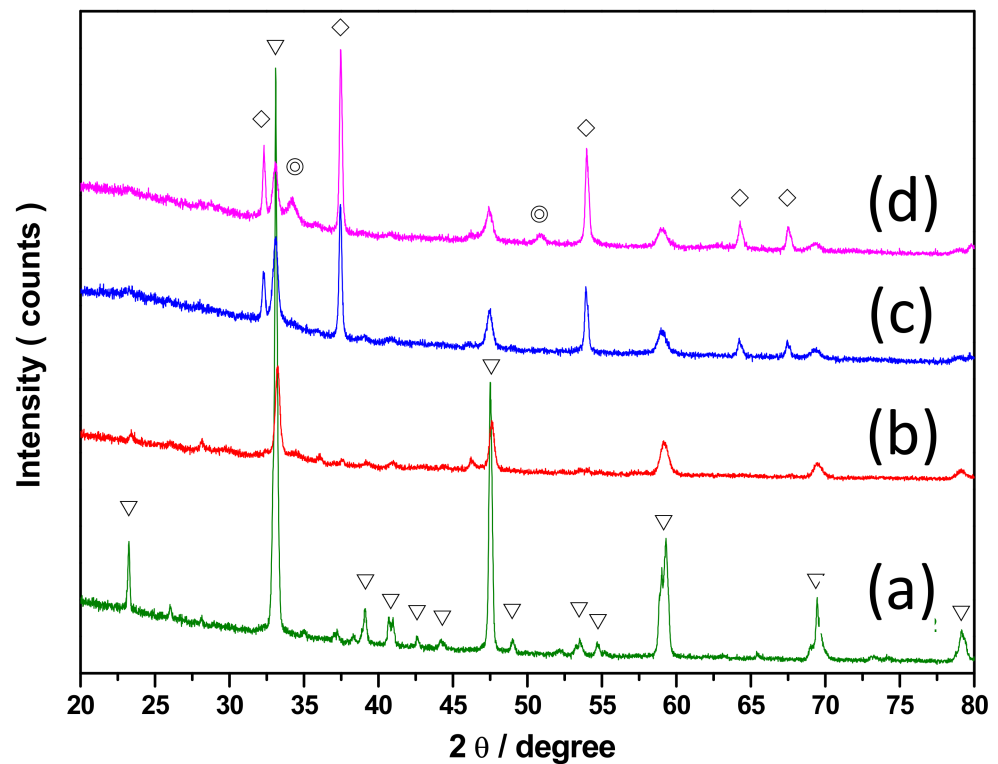


Figure 2. XRD result of as-prepared calcium-based sorbents: (a) CaTi-1.2, (b) CaTi-2, (c) CaTi-3, (d) CaTi-5. The inverted triangle symbol, diamond symbol, and circle symbol represent CaTiO_3 , CaO , and Ca(OH)_2 , respectively.

The nitrogen adsorption/desorption analysis results are shown in Figure 3. All four sorbents showed surface areas of 5–17 m^2/g (Table 1). Similar value indicated that calcium-precursor loading had little influence on the change in surface area. The appearance of hysteresis loops indicated a porous structure, possibly due to nanoparticle aggregation or stacking. The pore size distribution of the sorbents in this work, CaTi-2, CaTi-3, and CaTi-5, were primarily in the range from 2 to 10 nm, whereas CaTi-1.2 was mainly in the range from 8 to 22 nm (Figure S1).

3.2. CO_2 Capture Performance of Adsorbents

The CO_2 -capture performance of calcium-based sorbents is presented in Figure 4. All sorbents showed rapidly increasing capture in less than 3 min before reaching saturation. CO_2 capture by calcium oxide involved two stages: the first was a rapidly increasing capture amount controlled by chemical reaction, and the second was slowly increasing capture amount controlled by an inner-diffusion mechanism [6,13]. However, these calcium-based sorbents were mainly observed first rapidly increasing in the capture-amount stage, while the inner-diffusion stage was unclear. This result indicated that the calcium-oxide particle size in these sorbents was very small, so the calcium oxide in inner sites could be utilized easily. Wei et al. concluded that pore size located in the range from 2 to 10 nm is beneficial for the chemical reaction controlled stage [28]. Therefore, CaTi-3 and CaTi-5 more rapidly increased than the other two sorbents, which may be related to the reason that most of their pore sizes were in the range from 2 to 10 nm. The saturated capture amount increased with increased calcium-precursor loading because a higher amount of calcium oxide was present (Table 1).

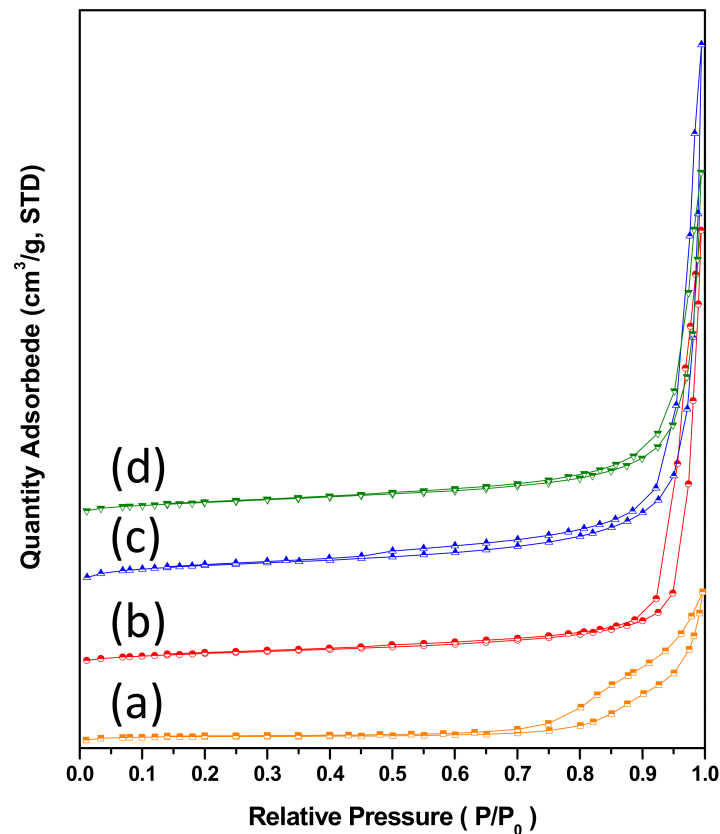


Figure 3. Nitrogen adsorption/desorption isotherm of as-prepared calcium-based sorbents: (a) CaTi-1.2, (b) CaTi-2, (c) CaTi-3, (d) CaTi-5.

Table 1. Surface area and CO₂ capture capacity of calcium-based sorbents.

Sorbent	Surface Area (m ² /g)	CO ₂ Capture Capacity (mmole CO ₂ /g Sorbent)
CaTi-1.2	5	0.2
CaTi-2	10	2.6
CaTi-3	17	7.0
CaTi-5	12	10.1

3.3. Multicycle Capture and Regeneration Experiment of Adsorbents

The sorbents with the highest and second highest saturated capture amounts, CaTi-3 and CaTi-5, were selected for evaluation of their multicycle stability. The results are shown in Figure 5a,b, respectively. After 20 cycles of repeated use, the capture capacity of CaTi-3 was almost unchanged, whereas that of CaTi-5 decreased by ~17% compared with that in the first cycle (Figure 5c). CaTi-5 showed capacity loss because too much calcium oxide was present in this sorbent. The carbonation behavior of CaTi-3 and CaTi-5 at the twentieth cycle were different than the first cycle (Figure 5d). The two stage carbonation behavior due to more importance of the inner-diffusion mechanism at the twentieth cycle in comparison to the first cycle carbonation reaction revealed that slight sintering occurred in both sorbents during 20 cycles of repeated use. The sintering phenomenon occurred at the CaCO₃ phase due to its low Tamman temperature (~530 °C) [13]. Thus, the inner-diffusion controlled mechanism became important as repeated times increased. This result indicated that after 20 cycles of repeated use, calcium species particle sizes increased. Additionally, the capture capacity of CaTi-3 in the twentieth-cycle carbonation was closer to its first cycle than the CaTi-5 case at 10 min, indicating that calcium species particles suffered a greater degree of sintering in CaTi-5 than in CaTi-3.

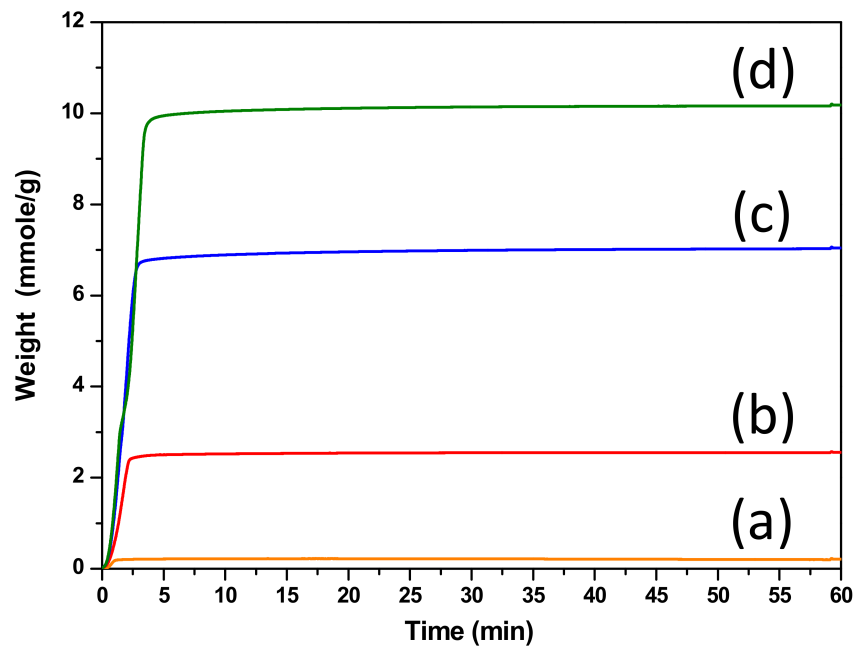


Figure 4. CO₂ capture performance of calcium-based sorbents: (a) CaTi-1.2, (b) CaTi-2, (c) CaTi-3, (d) CaTi-5.

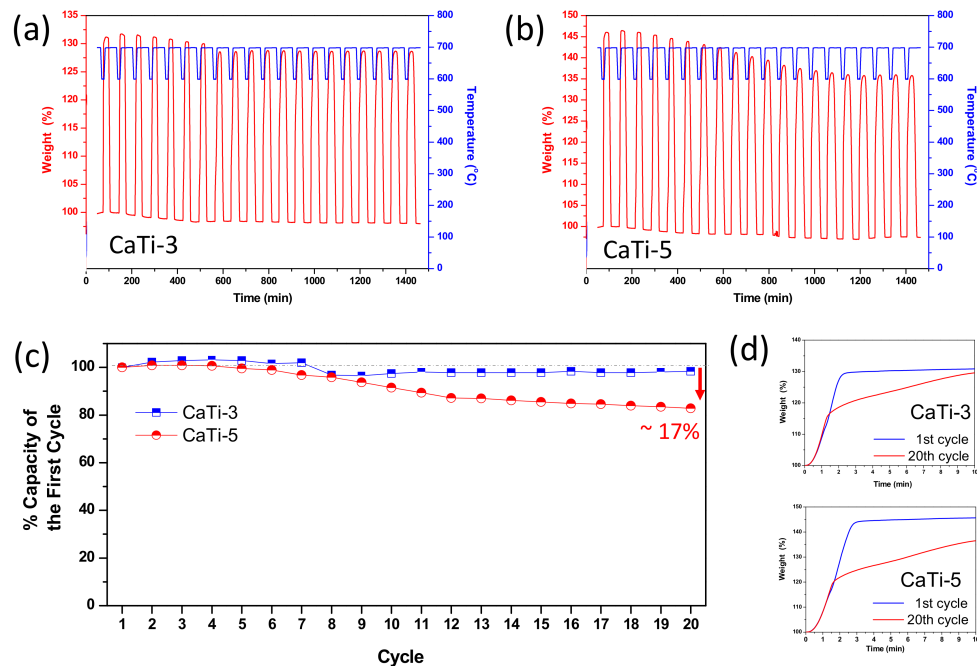


Figure 5. Twenty cyclic repeating experiment results of CaTi-3 (a) and CaTi-5 (b); percentage of capture capacity of each cycle to the first cycle (c), and the carbonation performance of the first and the twentieth experiment of CaTi-3 (up) and CaTi-5 (down) (d).

The XRD results of CaTi-3 and CaTi-5 sorbents after 1 and 20 cycles of repeated use are presented in Figure 6a,b, respectively. After 1 cycle, CaTiO₃ and Ca(OH)₂ diffraction signals could be found in both sorbents. However, several CaCO₃ diffraction signals (JCPDS 850849) clearly appeared in CaTi-5 after 20 cycles of repeated use. Given that the cycle experiment involved an initial carbonation part followed by regeneration, the CaCO₃ species remaining after the cyclic experiment indicated that decarbonation efficiency

decreased. The CaCO_3 species could not capture CO_2 , so CaTi-5-capture capacity loss occurred after 20 cycles. Moreover, one CaCO_3 diffraction signal with a very weak peak intensity was found in CaTi-3 after 20 cycles, indicating that cyclic stability started to decrease when the mole ratio of calcium to titanium was greater than 3. The SEM images of CaTi-3 and CaTi-5 after 20 cycles are shown in Figure 7. CaTi-5 presented a denser morphology than CaTi-3, indicating a lower carbonation performance of CaTi-5 compared to CaTi-3, which was consistent with the cyclic-experiment results.

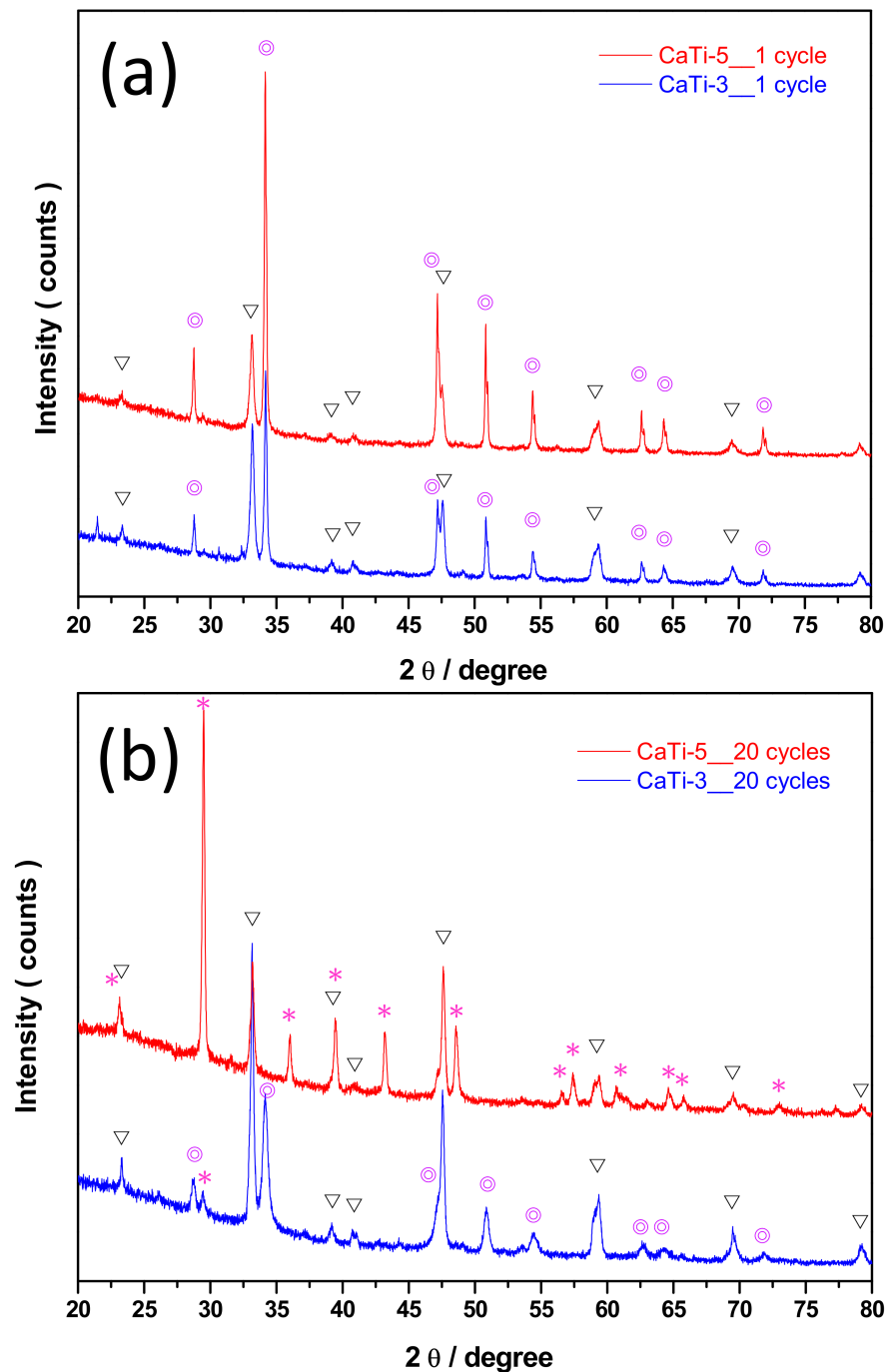


Figure 6. XRD results of (a) CaTi-3 and (b) CaTi-5 collected from after 1 cycle and 20 cycle experiments, where the invert triangle symbol represents CaTiO_3 , the circle symbol represents Ca(OH)_2 , and the star symbol represents CaCO_3 .

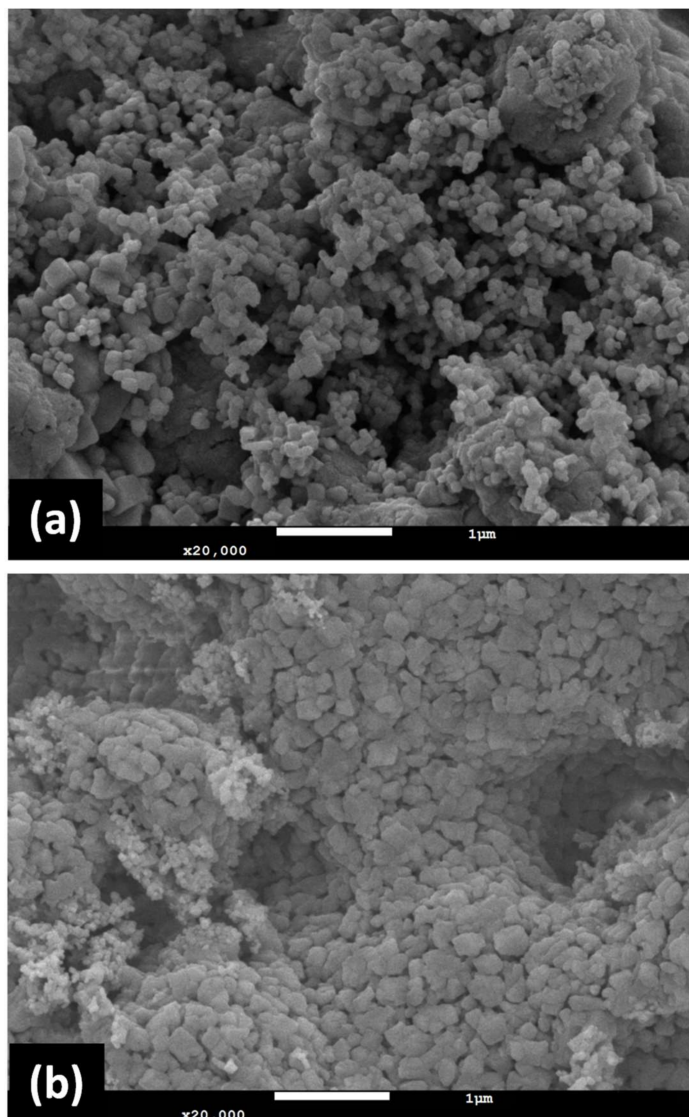


Figure 7. SEM images of CaTi-3 (a) and CaTi-5 (b) after 20 cycle experiment.

CaTi-3 was selected for further evaluation of its multicycle stability at high temperatures under CO₂ flowing regeneration conditions because of its superior cyclic performance (Figure 8). The results showed significant capacity loss at the third cycle, probably due to microstructure change, followed by a gradual increase in capacity, which may be related to structure optimization. After the seventh cycle, the capacity became unchanged and exhibited about a 32% decrease compared with the first cycle. The weight loss during regeneration was similar to weight gain during carbonation in each cycle. Thus, the capture capacity decreased after several times of repeated use, which may be related to low carbonation efficiency. Hence, CaO was not completely utilized at the end of carbonation. The XRD results of CaTi-3 after 1 and 10 cycles of repeated use showed diffraction signals attributed to CaTiO₃, CaCO₃, and CaO species (Figure 9). After one cycle, the diffraction signals due to CaTiO₃ and CaO species should have appeared at the end of regeneration. The diffraction signals assigned to CaCO₃ species was due to the reaction of some CaO with CO₂ as the experiment finished. The same situation occurred after 10 cycles. The SEM images of CaTi-3 showed more aggregated and fused morphology with increasing repetition times (Figure 10).

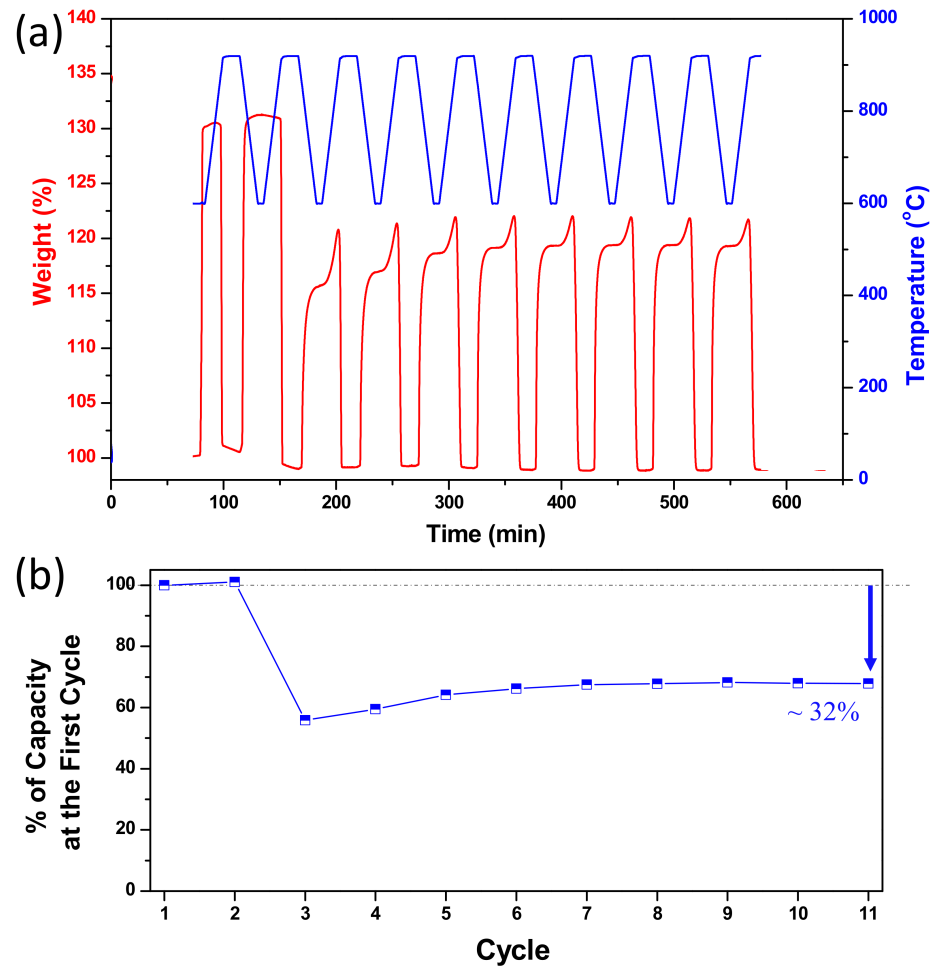


Figure 8. Ten cyclic repeating experiment results of CaTi-3 (a), and the percentage of capture capacity of each cycle to the first cycle (b).

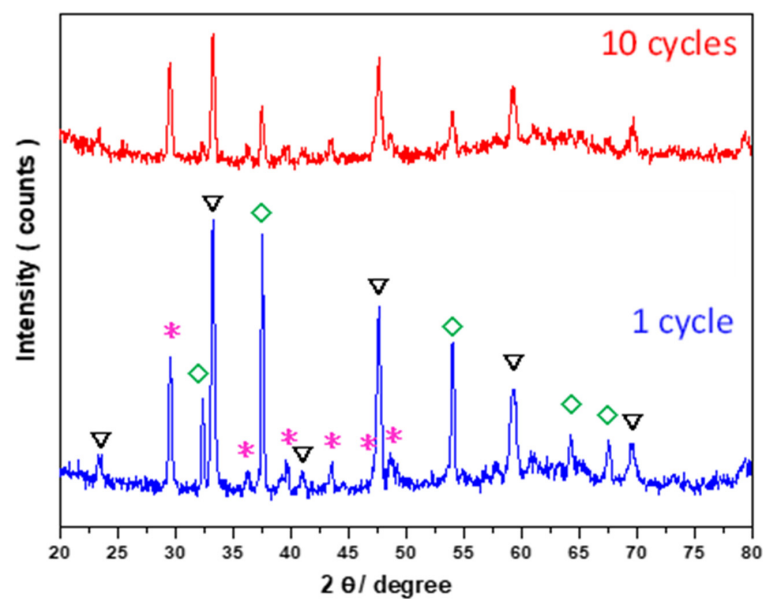


Figure 9. XRD results of CaTi-3 collected from after 1 cycle and 10 cycles experiment. Where the invert triangle symbol represents for CaTiO₃, the diamond symbol represents for CaO, the star symbol represents for CaCO₃.

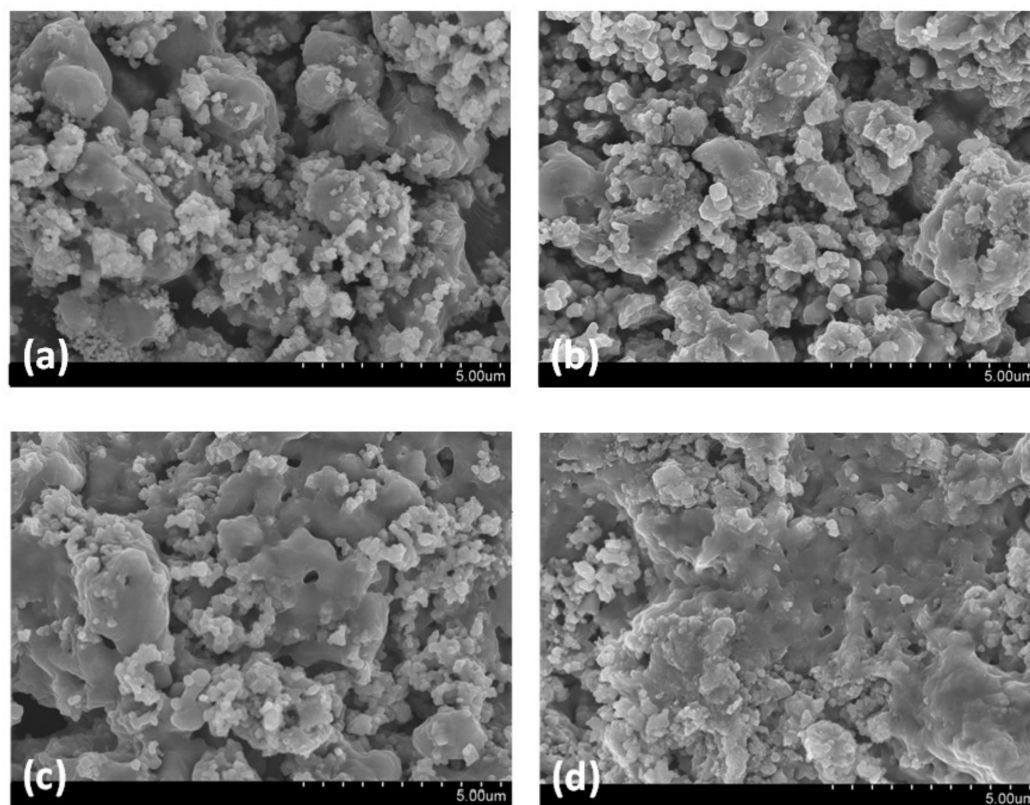


Figure 10. SEM images of CaTi-3 after (a) 1 cycle, (b) 2 cycle, (c) 3 cycle, and (d) 20 cycle experiments.

The different types of behavior of the CaTi-3 sorbent cyclic experiment under N_2 flowing at low temperatures ($700\text{ }^\circ\text{C}$ for 30 min, mild condition) or under CO_2 flowing at high temperatures ($920\text{ }^\circ\text{C}$ for 15 min, severe condition) may be related to calcium formation on the support surface based on the XRD results of sorbents collected after cyclic experiment (Figure 11). Under mild regeneration conditions, the cyclic experiment process mainly involves $Ca(OH)_2$ and $CaCO_3$ species transformation. $Ca(OH)_2$ is under the molten state (melting point $\sim 512\text{ }^\circ\text{C}$), while $CaCO_3$ is in the solid state (melting point $\sim 825\text{ }^\circ\text{C}$) during carbonation and regeneration. During carbonation, the ions diffuse in molten $Ca(OH)_2$ layers more efficiently; thus, almost all calcium species can be utilized. When $CaCO_3$ forms, it will precipitate due to its larger density ($2.71\text{ cm}^3/\text{g}$) than $Ca(OH)_2$ ($2.21\text{ cm}^3/\text{g}$). During regeneration, the molten $Ca(OH)_2$ layer permits the easy regeneration of $CaCO_3$ located in the interior position. Therefore, nearly no capture capacity decay occurs. Under severe regeneration conditions, the cyclic experiment process mainly involves CaO and $CaCO_3$ species transformation. $CaCO_3$ is in the solid state during carbonation and under the molten state during regeneration; furthermore, CaO is in the solid state, and sintering cannot occur during carbonation and regeneration (melting point $\sim 2613\text{ }^\circ\text{C}$, Tammann temperature $\sim 1154\text{ }^\circ\text{C}$) [29]. During carbonation, external CaO can react with CO_2 to form $CaCO_3$, whereas CO_3^{2-} and O^{2-} exchange occurs at the internal $CaCO_3/CaO$ interface [4]. During regeneration, CaO forms and precipitates in molten $CaCO_3$ (density of CaO is $3.34\text{ cm}^3/\text{g}$). The microstructure stacked by these aggregated precipitates will affect subsequent cycle carbonation reaction performance. More precipitants with densely stacked structures reduce the carbonation efficiency.

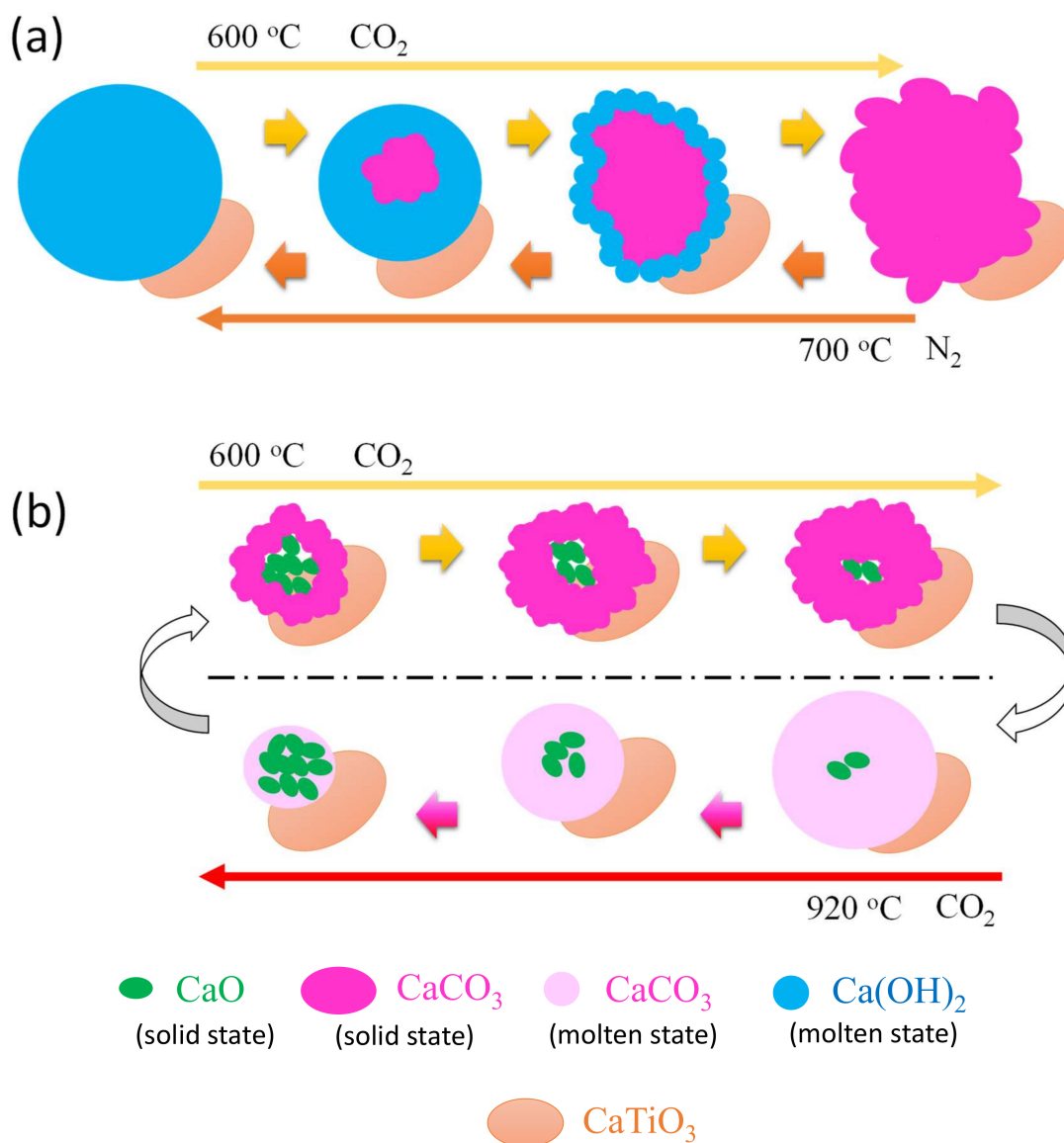


Figure 11. Schematic diagram of CaTi-3 under (a) mild regeneration conditions, and (b) severe regeneration of multicycle experiment.

4. Conclusions

We used a versatile aerosol-assisted self-assembly method to synthesize homogeneous CO₂ adsorbent with calcium and titanium. The calcium titanium oxide species (CaTiO₃) dispersed active species (CaO) well and mitigated the sintering effect during high-temperature multicycle carbonation and decarbonation. CO₂-capture capacity increased with increased mole ratios of calcium and titanium. With a ratio equal to 3, the CO₂-capture capacity became as large as 7 mmol/g with excellent reaction kinetics. Even after 20 cycles under mild regeneration conditions, the CO₂-capture performance of CaTiO₃-decorated CaO-based adsorbent was nearly retained with morphologies and structures unchanged. Moreover, after 10 cycles under severe regeneration conditions, the capture capacity still retained nearly 70% of the first cycle.

Supplementary Materials: The following is available online at <https://www.mdpi.com/article/10.3390/nano11123188/s1>, Figure S1: BJH pore size distribution result of calcium-based sorbents.

Author Contributions: Conceptualization, R.-W.C. and C.-J.L.; Data curation, R.-W.C. and C.-J.L.; Formal analysis, R.-W.C. and C.-J.L.; Investigation, R.-W.C.; Methodology, R.-W.C. and Y.-H.L.;

Writing—original draft, R.-W.C.; Writing—review and editing, C.-J.L. and Y.-H.L. All authors have read and agreed to the published version of the manuscript.

Funding: This research was funded by Ministry of Science and Technology, Taiwan, grant number 109-2116-M-002-035.

Institutional Review Board Statement: Not applicable.

Informed Consent Statement: Not applicable.

Data Availability Statement: The data presented in this study are available on request from the corresponding authors.

Conflicts of Interest: The authors declare no conflict of interest.

References

1. Krödel, M.; Landuyt, A.; Abdala, P.M.; Müller, C.R. Mechanistic understanding of CaO-based sorbents for high-temperature CO₂ capture: Advanced characterization and prospects. *ChemSusChem* **2020**, *13*, 6259–6272. [[PubMed](#)]
2. Sin, G.; Lee, J.; Karakoti, A.; Bahadur, R.; Yi, J.; Zhao, D.; AlBahily, K.; Vinu, A. Emerging trends in porous materials for CO₂ capture and conversion. *Chem. Soc. Rev.* **2020**, *49*, 4360–4404.
3. Yang, N.; Xue, R.; Huang, G.; Ma, Y.; Wang, J. CO₂ adsorption performance and kinetics of ionic liquid-modified calcined magnesite. *Nanomaterials* **2021**, *11*, 2614. [[CrossRef](#)] [[PubMed](#)]
4. Choi, S.; Drese, J.H.; Jones, C.W. Adsorbent materials for carbon dioxide capture from large anthropogenic point sources. *ChemSusChem* **2009**, *2*, 796–854. [[CrossRef](#)] [[PubMed](#)]
5. Radfarnia, H.R.; Sayari, A. A highly efficient CaO-based CO₂ sorbent prepared by a citrate-assisted sol–gel technique. *Chem. Eng. J.* **2015**, *262*, 913–920. [[CrossRef](#)]
6. Hu, Y.; Jia, Q.; Shan, S.; Li, S.; Jiang, L.; Wang, Y. Development of CaO-based sorbent doped with mineral rejects–bauxite-tailings in cyclic CO₂ capture. *J. Taiwan Inst. Chem. Eng.* **2015**, *46*, 155–159. [[CrossRef](#)]
7. Wang, N.; Feng, Y.; Liu, L.; Guo, X. Effects of preparation methods on the structure and property of Al-stabilized CaO-based sorbents for CO₂ capture. *Fuel Process. Technol.* **2018**, *173*, 276–284. [[CrossRef](#)]
8. Liu, F.Q.; Li, W.H.; Liu, B.C.; Li, R.X. Synthesis, characterization, and high temperature CO₂ capture of new CaO based hollow sphere sorbents. *J. Mater. Chem. A* **2013**, *1*, 8037–8044. [[CrossRef](#)]
9. Sun, H.; Parlett, C.M.A.; Isaacs, M.A.; Liu, X.; Adwek, G.; Wang, J.; Shen, B.; Huang, J.; Wu, C. Development of Ca/KIT-6 adsorbents for high temperature CO₂ capture. *Fuel* **2019**, *235*, 1070–1076. [[CrossRef](#)]
10. Xu, Y.; Ding, H.; Luo, C.; Zheng, Y.; Zhang, Q.; Li, X.; Sun, J.; Zhang, L. Potential synergy of chlorine and potassium and sodium elements in carbonation enhancement of CaO-based sorbents. *ACS Sustain. Chem. Eng.* **2018**, *6*, 11677–11684. [[CrossRef](#)]
11. Sun, P.; Grace, J.R.; Lim, C.J.; Anthony, E.J. The effect of CaO sintering on cyclic CO₂ capture in energy systems. *AIChE J.* **2007**, *53*, 2432–2442. [[CrossRef](#)]
12. Kierzkowska, A.M.; Pacciani, R.; Muller, C.R. CaO-based CO₂ sorbents: From fundamentals to the development of new, highly effective materials. *ChemSusChem* **2013**, *6*, 1130–1148. [[CrossRef](#)] [[PubMed](#)]
13. Naeem, M.A.; Armutlulu, A.; Imtiaz, Q.; Donat, F.; Schäublin, R.; Kierzkowska, A.; Müller, C.R. Optimization of the structural characteristics of CaO and its effective stabilization yield high-capacity CO₂ sorbents. *Nat. Commun.* **2018**, *9*, 2408–2418. [[CrossRef](#)] [[PubMed](#)]
14. Nityashree, N.; Manohara, G.V.; Maroto-Valer, M.M.; Garcia, S. Advanced high-temperature CO₂ sorbents with improved long-term cycling stability. *ACS Appl. Mater. Interfaces* **2020**, *12*, 33765–33774. [[CrossRef](#)]
15. Sun, J.; Guo, Y.; Yang, Y.; Li, W.; Zhou, Y.; Zhang, J.; Liu, W.; Zhao, C. Mode investigation of CO₂ sorption enhancement for titanium dioxide decorated CaO-based pellets. *Fuel* **2019**, *256*, 116009–116017. [[CrossRef](#)]
16. Radfarnia, H.R.; Iliuta, M.C. Metal oxide-stabilized calcium oxide CO₂ sorbent for multicycle operation. *Chem. Eng. J.* **2013**, *232*, 280–289. [[CrossRef](#)]
17. Guo, H.; Kou, X.; Zhao, Y.; Wang, S.; Sun, Q.; Ma, X. Effect of synergistic interaction between Ce and Mn on the CO₂ capture of calcium-based sorbent: Textural properties, electron donation, and oxygen vacancy. *Chem. Eng. J.* **2018**, *334*, 237–246. [[CrossRef](#)]
18. Huang, C.H.; Chang, K.P.; Yu, C.T.; Chiang, P.C.; Wang, C.F. Development of high-temperature CO₂ sorbents made of CaO-based mesoporous silica. *Chem. Eng. J.* **2010**, *161*, 129–135. [[CrossRef](#)]
19. Valverde, J.M.; Pontiga, F.; Soria-Hoyo, C.; Quintanilla, M.A.S.; Moreno, H.; Duran, F.J.; Espin, M.J. Improving the gas–solids contact efficiency in a fluidized bed of CO₂ adsorbent fine particles. *Phys. Chem. Chem. Phys.* **2011**, *13*, 14906–14909. [[CrossRef](#)]
20. Perez-Vaquero, J.; Valverde, J.M.; Quintanilla, M.A.S. Flow properties of CO₂ sorbent powders modified with nanosilica. *Powder Technol.* **2013**, *249*, 443–455. [[CrossRef](#)]
21. Gunathilake, C.; Jaroniec, M. Mesoporous calcium oxide–silica and magnesium oxide–silica composites for CO₂ capture at ambient and elevated temperatures. *J. Mater. Chem. A* **2016**, *4*, 10914–10924. [[CrossRef](#)]
22. Ammendola, P.; Raganati, F.; Miccio, F.; Murri, A.N.; Landi, E. Insights into utilization of strontium carbonate for thermochemical energy storage. *Renew. Energy* **2020**, *157*, 769–781. [[CrossRef](#)]

23. Raganati, F.; Chirone, R.; Ammendola, P. Calcium-looping for thermochemical energy storage in concentrating solar power applications: Evaluation of the effect of acoustic perturbation on the fluidized bed carbonation. *Chem. Eng. J.* **2020**, *392*, 123658–123668. [[CrossRef](#)]
24. Yu, C.; Kuo, H.; Chen, Y. Carbon dioxide removal using calcium aluminate carbonates on titanic oxide under warm-gas conditions. *Appl. Energy* **2016**, *162*, 1122–1130. [[CrossRef](#)]
25. Wu, S.F.; Zhu, Y.Q. Behavior of CaTiO₃/nano-CaO as a CO₂ reactive adsorbent. *Ind. Eng. Chem. Res.* **2010**, *49*, 2701–2706. [[CrossRef](#)]
26. Lin, C.J.; Yang, W.T. Ordered mesostructured Cu-doped TiO₂ spheres as active visible-light-driven photocatalysts for degradation of paracetamol. *Chem. Eng. J.* **2014**, *237*, 131–137. [[CrossRef](#)]
27. Fan, J.; Boettcher, S.W.; Stucky, G.D. Nanoparticle assembly of ordered multicomponent mesostructured metal oxides via a versatile sol-gel process. *Chem. Mater.* **2006**, *18*, 6391–6396. [[CrossRef](#)]
28. Wei, S.; Han, R.; Su, Y.; Gao, J.; Zhao, G.; Qin, Y. Pore structure modified CaO-based sorbents with different sized templates for CO₂ capture. *Energy Fuels* **2019**, *33*, 5398–5407. [[CrossRef](#)]
29. Rodaev, V.V.; Razlivalova, S.S. Performance and durability of the Zr-doped CaO sorbent under cyclic carbonation–decarbonation at different operating parameters. *Energies* **2021**, *14*, 4822. [[CrossRef](#)]